# Understanding phase contrast artefacts in micro computed absorption tomography

Erik L. G. Wernersson*, Matthieu N. Boone†, Jan Van den Bulcke‡, Luc Van Hoorebeke§, Cris L. Luengo Hendriks*
*Centre for Image Analysis, Box 337, SE-751 05, Uppsala
†Ghent University, Dept. of Geology and Soil Science, Krijgslaan 281, S8 9000 Ghent
‡Ghent University, Dept. of Forest and Water Management. Coupure Links, 653, 9000 Ghent
§ Ghent University, Dept. of Physics and Astronomy, Proeftuinstraat 86, 9000 Ghent

***Abstract*—Phase contrast imaging is a technique which captures objects with little or no light absorption. This is possible due to the wave nature of light, i.e., diffraction. In computerised tomography, the aim is most often to reconstruct the light absorption property of objects but many objects can not be imaged without obtaining a mix of both absorption and phase, this is especially true for weakly absorbing objects at high resolution.**

**Hence, phase contrast is usually considered an unwanted artefact which should be removed. Traditionally this is done directly on the projection data prior to the filtered back projection algorithm and the filter settings are derived from the physical setup of the imaging device.**

**In this paper we show how these operations can be carried out on the reconstructed data, without access to the projection images, which yields much flexibility over previous approaches. Especially, filtering can be applied to small regions of interest which simplifies fine tuning of parameters, and some low pass filtering can be avoided which is inherent in previous methods. We will also show the filter parameters can be estimated from step edges in the reconstructed images.**

## I. Introduction

In X-ray computed tomography (CT), the attenuation of X-rays is the main physical process. At high resolutions the phase shift of X-rays becomes an equally important effect, called phase contrast [1], [2]. The book by Liptson and Lipson [3] contains a good overview of the physics behind these phenomena and the book by Born and Wolf [4] is a standard reference for more advanced topics. Several methods have been developed to exploit this phase shift, such as grating-based phase retrieval [5], [6] and multiple-image holotomography [7], [8], where phase shift is visualized by in-line beam propagation. Similarly, beam propagation also creates phase contrast in standard micro-CT, where projections from multiple angles are used to create a three dimensional image of the object. In this case, it gives rise to edge enhancement [9], [10] and can as such be exploited [11], [12], but when the attenuation is of major interest it can become an unwanted feature.

This discussion will be limited to single-image in-line phase contrast imaging where both attenuation and phase shift occur, so-called mixed phase and amplitude data. Within this context, there are several methods that deal with projection images. The modified Bronnikov algorithm (MBA) [13], [14] and Paganin phase retrieval (PPR) [15] are the two most common phase-retrieval algorithms. Other algorithms have been proven to yield similar or worse results at experimental conditions discusses by Burvall et al. [16]. The Bronnikov aided correction (BAC) on the other hand, is a phase-correcting algorithm [17]. Because both MBA and PPR assume single-material objects, phase retrieval is equivalent to phase correction, the same applies to the proposed method in this paper. Due to the implementation of both algorithms, the reconstructed value represents the local attenuation coefficient, making both algorithms *de facto* phase-correcting [18].

Drawbacks with all current methods is that they are pre-processing methods that require access to projection data and tomographic reconstruction of the output data to evaluate parameters. We now propose a post-processing method that significantly decreases these processing times, which can also be used with commercial systems in which the reconstruction module is not available or the reconstruction module can not be modified, which is the case in some commercial systems or for non-expert users at imaging facilities such as synchrotron beamlines.

Artefacts are arguably best countered by the reconstruction method since only then can the reconstructed images be guaranteed to be consistent with the projection data. Post-processing is in a way blind to the reconstruction process, and thus more susceptible to false corrections. Even so, the ease of use makes post-processing methods popular, for example to reduce ring artefacts [19], [20] and to handle the typical cupping artefacts due to beam hardening [21].

To our knowledge there are no publications on phase artefact suppression without access to the projection data. In this paper it will be shown that it is possible to remove much of the phase artefacts in images after reconstruction once the corresponding parameters are determined. The parameters can be linked intuitively to the magnitude of the effect and the width of the ringing around edges. The method is qualitatively compared to the three pre-processing methods mentioned earlier, where a filter is applied on the projection data.

This is a shortened version of a previous paper [22] with the addition of section IV, which is new.

## II. Background

The relation between object and X-ray projection images is usually given by Beer's law, which describes the ratio of the X-ray intensity of an incoming beam $I_{\text{source}}$ and the attenuated ray $I_{\text{attenuated}}$ after it has passed through a sample by

$$\frac{I_{\text{attenuated}}}{I_{\text{source}}} = \exp\left(-\int_{p(s)} \mu \, ds\right), \tag{1}$$

where the integral is taken over a straight ray path, $p$, from the beam source to the detector plane $(x, y, z = 0)$ through the object described by a linear attenuation coefficient $\mu$.

The relation given by Eq. 1 is only valid for monochromatic X-rays and it is a geometrical approximation in the sense that a straight ray path is assumed. Consequently, a model with more detail is required to describe diffraction fringes or phase artefacts. The Transport of Intensity Equation (TIE) [23], [24], [25], gives a more detailed description of the relation and is the basis for most single-image phase contrast retrieval and removal algorithms [16].

At a sufficiently short propagation distance after the contact plane ($z = 0$), and assuming a slowly varying phase [2], the intensity $I$ evolves according to

$$\frac{\partial I(x,y,z)}{\partial z} = -\frac{\lambda}{2\pi}\nabla_\perp \left[I(x,y,z)\nabla_\perp \phi_0(x,y)\right], \tag{2}$$

where $\nabla_\perp$ is the Gradient operator orthogonal to the rays, $\phi_0(x,y) = \frac{2\pi}{\lambda}\int_p (1 - n(x,y,z))\, ds$ the phase modulation and $n$ is the real part of the refractive index.

An approximate solution can be found [9] even for cone beam CT with geometrical magnification, $S$[26]:

$$I(x,y,D) \approx I(x,y,0)\cdot \left[1 - \frac{\lambda D}{2\pi S}\nabla_\perp^2 \phi + \frac{\lambda D}{2\pi S}\left(\frac{\partial \mu_0}{\partial x}\frac{\partial \phi_0}{\partial x} + \frac{\partial \mu_0}{\partial y}\frac{\partial \phi_0}{\partial y}\right)\right], \tag{3}$$

where $D$ is the propagation distance and $\mu_0 = \int_p \mu(x,y,z)ds$. It must be noted that these equations are only valid for a monochromatic X-ray beam, an effective energy can be defined analogous to attenuation-based X-ray CT.

Following [27], the last terms of Eq. 3 is assumed to be relatively small and can be neglected. Since the Laplacian and the filtered back projection are commuting operators, it can be shown that the reconstructed attenuation coefficient is approximately [27]

$$\mu_{\text{reconstructed}}(\mathbf{x}) = \mu(\mathbf{x}) + D\Delta n(\mathbf{x}), \tag{4}$$

where $\mathbf{x}$ denotes the three dimensional coordinate in the reconstructed volume.

For objects consisting of a single materials (and air) $n$ can be set proportional to $\mu$ without knowing the actual values. Note that this does not require that the object is of constant density.

The term $D\Delta n(\mathbf{x})$ is band limited, otherwise the fringes would have infinite amplitude and no width. In practice, there are several band limiting components, a detailed discussion on this topic can be found in Gureyev et al. [2]. With that taken into consideration, the following model is obtained for the reconstructed images:

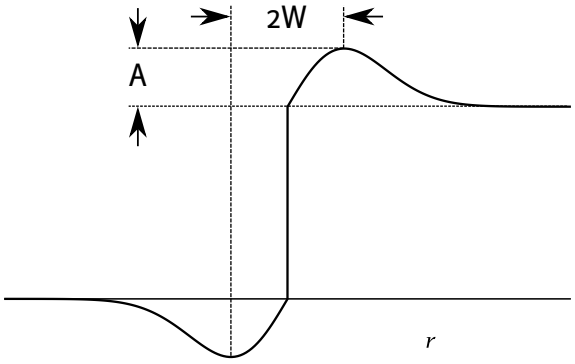


Fig. 1. Eq. 10 plotted along $r$ to illustrate the variables, $A = 1 - \max R$ and $W$, half the distance between $\min R$ and $\max R$. Compare with experimental data in Fig. 2

$$\mu_{\text{reconstructed}}(\mathbf{x}) = \mu(\mathbf{x}) + c\Delta_\sigma \mu(\mathbf{x}), \tag{5}$$

where $\Delta_\sigma(\mathbf{x}) = \Delta G_\sigma(\mathbf{x})$, $G_\sigma$ is a Gaussian kernel with standard deviation $\sigma$ and $c \in \mathbb{R}$.

## III. Removal of phase artefact by deconvolution

The model of Eq. 5 can be expressed as a convolution equation by

$$\mu_{\text{reconstructed}} = (\delta + c\Delta_\sigma) * \mu, \tag{6}$$

where $*$ denotes three-dimensional convolution operator and $\delta$ is the three dimensional Dirac delta function. As long as $c/\sigma^2 < e/2$, the relation can be inverted to obtain a filter which then provides the corrected image. If $\mathcal{F}$ denotes the Fourier transform, the absorption image is given as

$$\mu = \mathcal{F}^{-1}\left\{\mathcal{F}\left\{\mu_{\text{reconstructed}}\right\}/\mathcal{F}\left\{\delta + c\Delta_\sigma\right\}\right\}. \tag{7}$$

## IV. Parameter selection

The parameters could be derived from the setup directly. But since we assume no access to either projection images or the imaging protocol, we will derive them from the images.

Let $R$ be the reconstructed image, $G$ a three dimensional isotropic normal distribution, i.e.

$$G(\mathbf{x}) = |2\pi\Sigma|^{-1/2}\exp\left(-1/2(\mathbf{x}-\mu)^T\Sigma(\mathbf{x}-\mu)\right), \tag{8}$$

where $\mu = (0,0,0)^T$ and $\Sigma = \text{diag}(\sigma^2, \sigma^2, \sigma^2)$ and

$$\theta(\mathbf{x}) = \begin{cases} 1, & x_1 \geq 0, \\ 0, & x_1 < 0. \end{cases} \tag{9}$$

Inserted in Eq. 4 we get

$$R(\mathbf{x}) = \theta(x_1) + \epsilon\Delta G(\mathbf{x})_\sigma * \theta(x_1), \quad \epsilon < 0 \tag{10}$$

We will derive two functions: amplitude $A(\sigma, \epsilon)$ and width, $W(\sigma, \epsilon)$ according to Fig. 1.

To simplify, we will now rewite $G(\mathbf{x})$ as a function of radius in a spherical coordinate system i.e. let $r = (\mathbf{x}^T\mathbf{x})^{1/2}$, then

$$G(r) = \frac{1}{(2\pi\sigma^2)^{(3/2)}} \exp\left(-\frac{r^2}{2\sigma^2}\right). \quad (11)$$

and the Laplacian is (the derivatives with respect to $\theta$ and $\phi$ are zero)

$$\Delta G(r) = \frac{1}{r^2}\frac{\partial}{\partial r}\left(r^2 \frac{\partial G}{\partial r}\right). \quad (12)$$

Let $A = \left(2\pi\sigma^2\right)^{-3/2}$ and $B = -(2\sigma^2)^{-1}$, then

$$\Delta G(r) = \left(6AB + 4AB^2 r^2\right)\exp(Br^2) \quad (13)$$

$$= \frac{2\pi}{(2\pi\sigma^2)^{5/2}}\left(\frac{r^2}{\sigma^2} - 3\right)\exp(-\frac{r^2}{2\sigma^2}) \quad (14)$$

$$= (C + r^2 D)\exp(Br^2) \quad (15)$$

where

$$C = \frac{-3}{(2\pi)^{3/2}(\sigma^2)^{5/2}}, \quad D = \frac{1}{(2\pi)^{3/2}(\sigma^2)^{7/2}}. \quad (16)$$

The amplitude can be expressed as the max of the integral

$$A(\sigma) = \max\ A(z_m, \sigma) \quad (17)$$

$$= \max\ -\epsilon \int_0^{z_m(\sigma)} P(z)\mathrm{d}z, \quad z_m(\sigma) > 0, \quad (18)$$

where

$$P(z) = \int_{-\infty}^{\infty}\int_{-\infty}^{\infty} \Delta G(x, y, z)\mathrm{d}x\mathrm{d}y \quad (19)$$

i.e. the max of the convolution $\epsilon\Delta G * \theta(\mathbf{x})$ and similarly, the width, $W$ of the fringes is

$$W = \arg\ \max\ A(z_m, \sigma) \quad (20)$$

It is clear that $W$ is independent on any constant multiples before $\Delta G$, as seen in Eq. 18.

The following two identities:

$$\int x^2 \exp(-\alpha x^2)\mathrm{d}x = \frac{\sqrt{\pi}}{2\alpha^{3/2}}, \quad \alpha > 0 \quad (21)$$

$$\int \exp(-\alpha x^2)\mathrm{d}x = \frac{\sqrt{\pi}}{\sqrt{\alpha}}, \quad \alpha > 0 \quad (22)$$

are used to carry out the integrals in $x$ and $y$ and yields:

$$A(\sigma) = \max -2\pi A \int_0^{z_m} (1 + 2ABz^2)\exp(Bz^2)\mathrm{d}z \quad (23)$$

which gives $z_m = \sqrt{\frac{-1}{2B}} = \sigma$.

And finally, using the following identities:

$$\int_0^{\sigma} \exp(Bz^2)dz = \frac{\sqrt{\pi}\mathrm{erf}\left(\sigma\sqrt{-B}\right)}{2\sqrt{-B}} \quad (24)$$

$$\int_0^{\sigma} z^2 \exp(Bz^2)dz = \frac{\sqrt{\pi}\mathrm{erf}\left(\sigma\sqrt{-B}\right)}{4(-B)^{3/2}} + \frac{\sigma\exp\left(B\sigma^2\right)}{2B} \quad (25)$$

the error functions cancel out and we arrive at:

$$\begin{cases} A(\sigma, \epsilon) &= \frac{\epsilon}{\sigma^2 \exp(1/2)\sqrt{2\pi}}, \\ W(\sigma, \epsilon) &= \sigma, \end{cases} \quad (26)$$

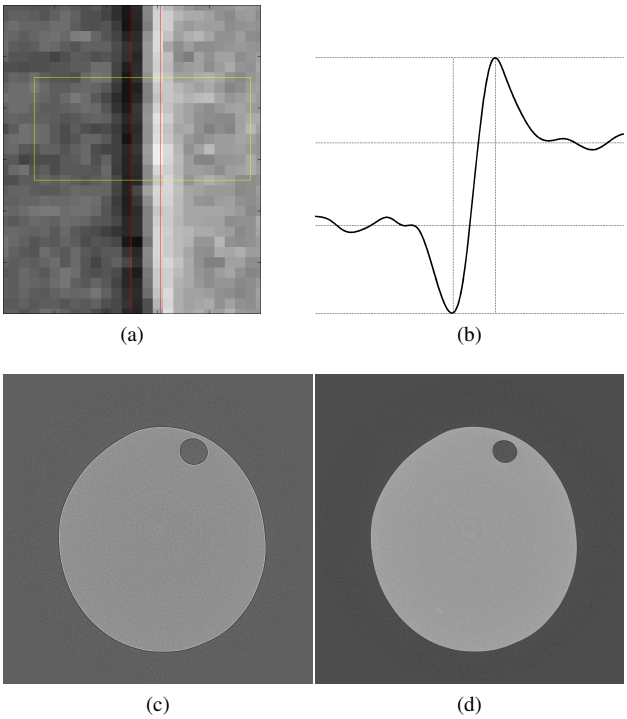

Fig. 2. a) An edge in a CT image. b) Pixel values across an edge in an image, slightly averaged orthogonal to the line. c) A slice prior filtering d) a slice after filtering with parameters estimated from (a).

i.e.

$$\begin{cases} \sigma(W, A) &= W, \\ \epsilon(W, A) &= AW^2\sqrt{2\pi}\exp(1/2). \end{cases} \quad (27)$$

Note that a step edge of height 1 was used and that scaling will be required in most cases with CT data.

There are numerical aspects to take into consideration in practical applications. The filter will not sample well when $\sigma < 1$. A real example is shown in Fig. 2.

## V. Experiments

The filter will be demonstrated using both synthetic and experimental data. The synthetic dataset contains 1800 projection images of size $512 \times 512$ pixels and is obtained by a ray-tracing tool [28] and Eq. 3 for phase simulation. The phantom consists of a large sphere with a certain attenuation coefficient $\mu_1$ and refractive index decrement $\delta_1$. The large sphere contains 4 spherical holes ($\mu = \delta = 0$) of different size, and similarly 4 spherical inclusions with $\mu_2 = 2\mu_1$ and $\delta_2 = 2\delta_1$. Sample properties were chosen to achieve a minimum transmission of 90%, and a realistic amplitude of the phase effect. Poisson noise was added for a flat-field of 20,000 counts.

Experimental data of a wood sample with nutrient medium (malt extract agar) [29] was acquired at the UGCT nanoscanner setup, using a Hamamatsu L1711 open-type nanofocus X-ray source, operated at a tube voltage of $50\,kV_p$ and a tube current of $100\,\mu A$. Images are recorded using a Photonic Science VHR detector operated in binning 4 mode, resulting in an effective pixel pitch of $29.6\,\mu m$. With a source-to-object distance of $3.29\,mm$ and a object-to-detector distance of $161\,mm$, a geometrical magnification of approximately

| Method | NRMSE |
|---|---|
| FBP | $1.011 \pm 0.089$ |
| MBA | $1.054 \pm 0.003$ |
| PPR | $0.094 \pm 0.004$ |
| BAC | $0.247 \pm 0.012$ |
| SPR | $0.094 \pm 0.005$ |

TABLE I
NORMALISED ROOT MEAN SQUARE ERROR (NRMSE) OF RECONSTRUCTIONS FROM A PHANTOM IMAGE (SEE FIG. 3). THE VALUES ARE CALCULATED PER SLICE AND THEN AVERAGED.

50 resulted in a voxel side length of $0.591\,\mu m$ in the reconstructed volume. In total, 800 projection images of $970 \times 800$ pixels were taken at an exposure time of $2000\,ms$ per image. Images were reconstructed using the UGCT developed software package Octopus (inCT [30], http://www.inCT.be) which includes a phase artefact module to perform reconstructions using the MBA, BAC and PPR filter.

The filter in Eq. 7 was implemented and run in Matlab (The MathWorks, Natick, MA, USA). To filter a 3D ROI of $100 \times 100 \times 100$ pixels took $0.5\,s$ and to filter a volume of $1000 \times 1000 \times 1000$ pixels took 3 minutes on a system with four Intel Xeon X5650 CPUs and 120 GB RAM. Filters have been applied in 3D, but in the following sections evaluated on 2D slices.

For the heuristic parameter selection, $c_0 = -10, \delta_c = 10$ and $\sigma_0 = 1, \delta_\sigma = 0.5$ have been used as initial settings. The parameters $\delta_c$ and $\delta_\sigma$ have been decreased by a factor 0.7 each time. Convergence has been obtained after 10 to 20 iterations.

All images shown in the paper are stretched in intensity to use the full dynamic range available in the print. The lowest value is mapped to black and the highest value is mapped to white. This cause the visual contrast to be decreased when more extreme values are present, as is the case with phase fringes.

## VI. RESULTS

The experiments on synthetic data are presented in Fig. 3 and errors for the reconstructed volume compared to the simulated phantom are compiled in Table I. In Fig. 3-a the phantom is shown after FBP and in Fig. 3-b the same image is shown after manual parameter selection and application of SPR. Fig. 3-c shows line profiles through the images where it can be seen that the phase artefacts were removed. Due to the small $\sigma$ there is no clear separation between phase artefact and noise so some noise was removed as well. For comparison, all methods where used to remove phase artefacts from the sample. The normalized mean square errors are compiled in Table I.

In Fig. 4, a comparison of the different techniques is shown. Fig. 4-a shows a filtered backprojection (FBP) reconstruction where phase artefacts can be seen at the edges, resulting in artificially increased gray values of the material and decreased, negative gray values in the air. Fig. 4-b and 4-c show the pre-processing phase retrieval methods MBA and PPR, respectively. A clear reduction

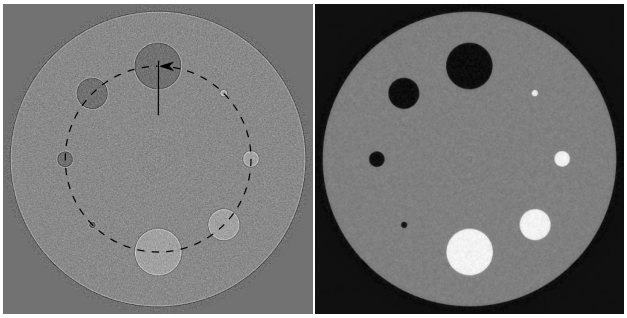

(a) FBP (b) SPR, $\sigma = 0.35$, $c = -4.5$

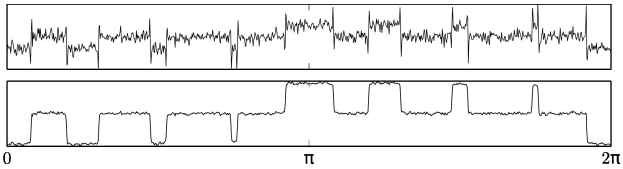


(c) 1D profiles through the samples as in Fig. a. Top: Fig. a, Bottom: Fig. b

Fig. 3. Phase artefacts removal from a phantom using SPR. a-b: slice number 256, of size $512 \times 512$ pixels, c: line profiles through the slices. The reference image is not shown but looks very similar to the image in b.

of phase effects and noise can be observed. The result of the phase-correction BAC method is shown in Figure 1d, where phase artefacts are successfully reduced. Fig. 4-e shows the result of the proposed post-processing method. Although random noise is apparently increased, the phase effects have been successfully eliminated. Note that no noise has been added, since the magnitude of the filter is less than 1 in the Fourier domain. Both MBA and PPR suppress high frequencies; so, to aid visual comparisons, the result of SPR has been low-pass filtered in Fig. 4-f. The experiment shows that SPR is capable of removing the phase effect from the sample without removing the noise, as well as producing results visually equal to those of PPR by the addition of a noise filter. It should be noted that the difference in gray value between nutrient medium and air is present already in Fig. 4-a, but is barely visible since the phase artefacts are much larger in magnitude.

## VII. DISCUSSION

It has been demonstrated that phase artefacts and absorption can be separated even after reconstruction by using SPR. The error estimates in Table I for the image in Fig, 3 shows that the performance can be almost identical to that of PPR. The theoretical assumptions made for both methods, i.e. monochromatic X-rays and a single-material object are less stringent than they appear, since phase-contrast imaging is often applied on low-attenuating samples where $\mu$ and $\delta$ behave very similar as a function of energy and material composition. For multi-material objects, an interface-specific approach as proposed by Beltran et al. [31], [32] can be applied, where parameters are optimized for each interface separately.

To obtain the filter parameters, a heuristic method has been used. It requires prior knowledge or assumption on the variation of the attenuation coefficient. Locations at

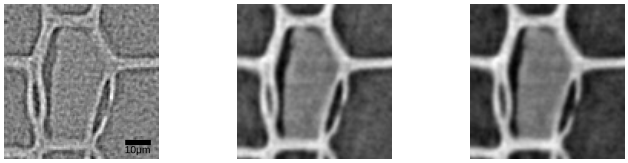

(a) FBP (b) MBA (c) PPR

(d) BAC (e) SPR, $\sigma = 1.2$, $c = -50$ (f) SPR & LP, $s = 1$

Fig. 4. a: A slice from a CT image of a sample with wood (the bright structure), nutrition medium (in the middle cell) and air (dark regions corresponds to air). b-f: filtered to remove phase artefacts. LP denotes a Gaussian low pass filter with standard deviation $s$ and SPR the method introduced in this paper. Corresponding histograms are shown in Fig. 6

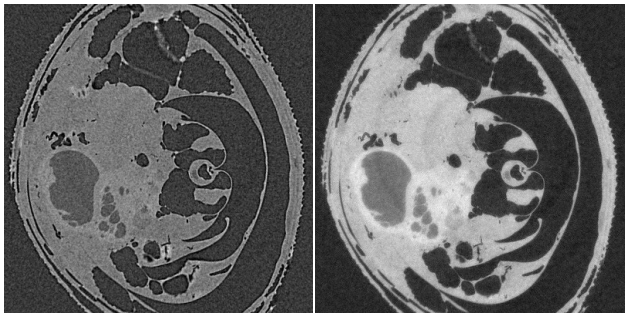

(a) A wasp. (b) Filtered, $\sigma = 0.85$, $c = -4$, $s = 1$.

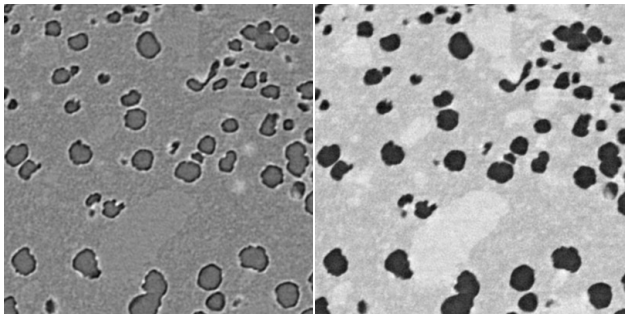

(c) A tablet (FBP, $s = 1$). (d) Filtered, $\sigma = 1.4$, $c = -17$, $s = 1$.

Fig. 5. Examples of filtering on different data sets.

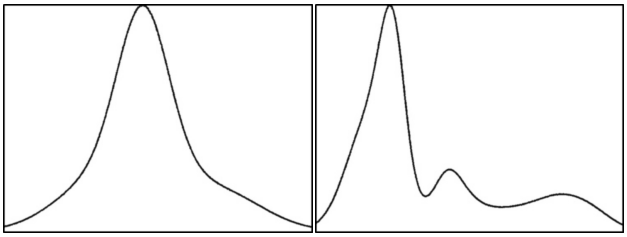

(a) FBP (b) MBA

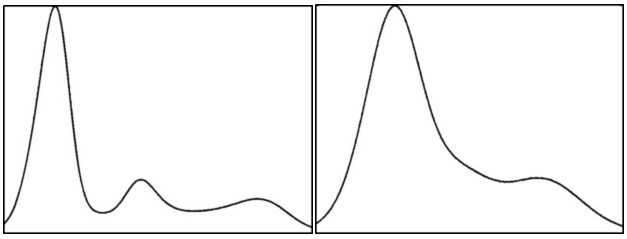

(c) PPR (d) BAC

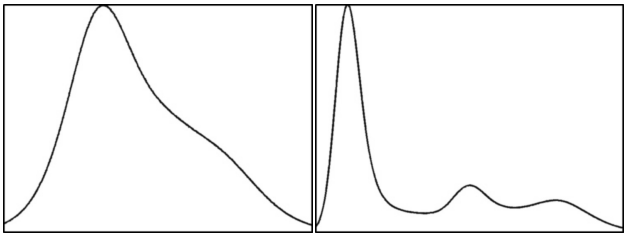

(e) SPR, $\sigma = 1.2$ $c = -50$ (f) SPR & LP, $\sigma = 1$

Fig. 6. Histograms of the volumes corresponding to the slices shown in Fig. 4. For the visualisation, the histograms are scaled from 0.5th to 99.5th percentile on horizontal axes and from 0 to max count on vertical axes. Note that, in this situation, BAC also would benefit from additional low pass filtering.

the interface between two materials are useful since a step edge variation usually can be assumed.

It should be noted that the objective of this method is to remove the phase artefact, and not to retrieve the optimal absorption. Weakly absorbing samples with low signal to noise ratio might benefit from noise filtering. It has been indicated before that MBA serves as a noise filter [13], [33], [34] and Fig. 4 indicates that also PPR removes noise. SPR will also remove high frequency noise for low values of $c$. It is trivial to include low-pass filtering in the inverse filter. Histograms are shown in Fig. 6 for the volumes in Fig. 4. Only one peak can be seen after FBP and SPR but after an additional low pass filtering, SPR produces three peaks just as MBA and PPR. Note that the x-axes are scaled differently.

A thorough discussion of noise reduction methods is beyond the scope of this article but it should be noted that non-linear noise reduction methods have shown the best performance in many situations [35], [36]. If any such methods are to be used, it is important that the image is not already low pass filtered. This is avoided with SPR when the fringes are wide, i.e. $\sigma$ far from 0.

## VIII. Conclusions

In this paper, we have proposed a post-processing filter to reduce phase artefacts on standard micro-CT data where they often hinder proper image analysis and can lead to false conclusions. This filter is derived using the same limitations on sample composition and X-ray spectrum, and yields results comparable to common single-image in-line phase retrieval and phase correction algorithms. Nevertheless, access to projection data is no longer required, and the filter can be applied prior to any image analysis. This makes phase correction accessible to non-expert users who don't have access to projection data or reconstruction software.

## ACKNOWLEDGMENT

The author would like to thank Gunilla Borgefors and Anders Brun their encouragement and interest in this project.

## REFERENCES

[1] T. J. Davis, D. Gao, T. E. Gureyev, A. W. Stevenson, and S. W. Wilkins, "Phase-contrast imaging of weakly absorbing materials using hard x-rays," *Nature*, vol. 373, pp. 595–598, 1995.

[2] T. E. Gureyev, Y. I. Nesterets, A. W. Stevenson, P. R. Miller, A. Pogany, and S. W. Wilkins, "Some simple rules for constant, signal-to-noise and resolution in in-line x-ray phase-contrast imaging," *Optics Express*, vol. 16, pp. 3223–3241, 2008.

[3] S. G. Lipson and H. Lipson, *Optical Physics*. Cambridge University Text, 1981.

[4] M. Born and E. Wolf, *Principles of optics 7th ed.* Cambridge University press, 1999.

[5] F. Pfeiffer, C. Kottler, O. Bunk, and C. David, "Hard X-ray phase tomography with low-brilliance sources," *Phys. Rev. Lett.*, vol. 98, p. 108105, 2007.

[6] C. David, T. Weitkamp, F. Pfeiffer, A. Diaz, J. Bruder, T. Rohbeck, A. Groso, O. Bunk, M. Stampanoni, and P. Cloetens, "Hard x-ray phase imaging and tomography using a grating interferometer," *Spectrochimica Acta, Part B: Atomic Spectroscopy*, vol. 62, pp. 626–630, 2007. [Online]. Available: http://dx.doi.org/10.1016/j.sab.2007.03.001

[7] P. Cloetens, W. Ludwig, J. Baruchel, D. V. Dyck, J. V. Landuyt, J. Guigay, and M. Schlenker, "Holotomography: Quantitative phase tomography with micrometer resolution using hard synchrotron radiation x rays," *Applied Physics Letters*, vol. 75, no. 19, pp. 2912–2914, 1999.

[8] M. Langer, P. Cloetens, and F. Peyrin, "Fourier-wavelet regularization of phase retrieval in x-ray in-line phase tomography," *J. Opt. Soc. Am. A*, vol. 26, no. 8, pp. 1876–1881, 2009.

[9] S. W. Wilkins, T. E. Gureyev, D. Gao, A. Pogany, and A. W. Stevenson, "Phase-contrast imaging using polychromatic hard x-rays," *Nature*, vol. 384, pp. 335–338, 1996.

[10] T. E. Gureyev, S. C. Mayo, D. E. Myers, Y. Nesterets, D. M. Paganin, A. Pogany, A. W. Stevenson, and S. W. Wilkins, "Refracting Röntgen's rays: Propagation-based x-ray phase contrast for biomedical imaging," *Journal of Applied Physics*, vol. 105, 2009.

[11] C. M. Laperle, T. J. Hamilton, P. Wintermeyer, E. J. Walker, D. Shi, M. A. Anastasio, Z. Derdak, J. R. Wands, G. Diebold, and C. Rose-Petruck, "Low density contrast agents for x-ray phase contrast imaging: the use of ambient air for x-ray angiography of excised murine liver tissue," *Phys. Med. Biol.*, vol. 53, no. 23, pp. 6911–6923, 2008.

[12] S. Matsuo, H. Fujita, J. Morishita, T. Katafuchi, C. Honda, and J. Sugiyama, "Preliminary evaluation of a phase contrast imaging with digital mammography," in *Digital Mammography / IWDM'08*. Springer, 2008, pp. 130–136.

[13] A. V. Bronnikov, "Theory of quantitative phase-contrast computed tomography," *J. Opt. Soc. Am. A*, vol. 19, no. 3, pp. 472–480, 2002.

[14] A. Groso, R. Abela, and M. Stampanoni, "Implementation of a fast method for high resolution phase contrast tomography," *Optics Express*, vol. 14, no. 18, pp. 8103–8110, 2006.

[15] D. Paganin, S. C. Mayo, T. E. Gureyev, P. R. Miller, and S. W. Wilkins, "Simultaneous phase and amplitude extraction from a single defocused image of a homogeneous object," *Journal of Microscopy*, vol. 206, no. 1, pp. 33–40, 2002.

[16] A. Burvall, U. Lundström, P. A. C. Takman, D. H. Larsson, and H. M. Hertz, "Phase retrieval in x-ray phase-contrast imaging suitable for tomography," *Optical Express*, vol. 19, no. 11, pp. 10 359–10 376, 2011.

[17] Y. De Witte, M. Boone, J. Vlassenbroeck, M. Dierick, and L. Van Hoorebeke, "The Bronnikov aided correction for x-ray computed tomography," *Journal of the Optical Society of America A*, vol. 26, no. 4, pp. 890–894, 2009.

[18] M. N. Boone, W. Devulder, M. Dierick, L. Brabant, E. Pauwels, and L. V. Hoorebeke, "Comparison of two single-image phase-retrieval algorithms for in-line x-ray phase-contrast imaging," *J. Opt. Soc. Am. A*, vol. 29, no. 12, pp. 2667–2672, 2012.

[19] M. Axelsson, S. Svensson, and G. Borgefors, "Reduction of ring artefacts in high resolution x-ray microtomography images," in *DAGM Symposium on Pattern Recognition, Berlin*. Springer, 2006, pp. 61–70.

[20] D. Prell, Y. Kyriakou1, and W. A. Kalender, "Comparison of ring artifact correction methods for flat-detector CT," *Physics in Medicine and Biology*, vol. 54, no. 12, pp. 3881–3895, 2009.

[21] P. M. Joseph and C. Ruth, "A method for simultaneous correction of spectrum hardening artifacts in CT images containing both bone and iodine," *Medical Physics*, vol. 24, no. 10, pp. 1629–1634, 1997.

[22] E. L. G. Wernersson, M. N. Boone, J. Van den Bulcke, L. Van Hoorebeke, and C. L. Luengo Hendriks, "Postprocessing method for reducing phase effects in reconstructed microcomputed-tomography data," *JOSA A*, vol. 30, pp. 455–461, 2013.

[23] M. R. Teague, "Deterministic phase retrieval: a green's function solution," *Journal of the Optical Society of America*, vol. 73, no. 11, pp. 1434–1441, 1983.

[24] ——, "Image formation in terms of the transport equation," *Optical Society of America*, vol. 2, no. 11, pp. 2019–2026, 1985.

[25] S. C. Mayo, P. R. Miller, S. W. Wilkins, T. J. Davis, D. Gao, T. E. Gureyev, D. Paganin, D. J. Parry, A. Pogany, and A. W. Stevenson, "Quantitative x-ray projection microscopy: phase-contrast and multi-spectral imaging," *Journal of Microscopy*, vol. 207, pp. 79–96, 2002.

[26] A. Peterzol, A. Olivo, L. Rigon, S. Pani, and D. Dreossi, "The effects on the imaging system on the validity limits of the ray-optical approach to phase contrast imaging," *Med. Phys*, vol. 32, no. 12, pp. 3617–3727, 2005.

[27] P. Cloetens, M. Pateyron-Salomé, J. Buffière, G. Peix, J. Baruchel, F. Peyrin, and M. Schlenker, "Observation of microstructure damage in materials by phase sensitive radiography and tomography," *J. Appl. Phys.*, vol. 81, no. 9, pp. 5878–5886, 1997.

[28] Y. De Witte, "Improved and practically feasible reconstruction methods for high resolution x-ray tomography," Ph.D. dissertation, Ghent University, 2010. [Online]. Available: http://lib.ugent.be/fulltxt/RUG01/001/404/410/RUG01-001404410_2010_0001_AC.pdf

[29] J. Van den Bulcke, M. Boone, J. Van Acker, and L. Van Hoorebeke, "Three-dimensional x-ray imaging and analysis of fungi on and in wood," *Microscopy and Microanalysis*, vol. 15, no. 5, pp. 395–402, 2009.

[30] J. Vlassenbroeck, M. Dierick, B. Masschaele, V. Cnudde, L. Van Hoorebeke, and P. Jacobs, "Software tools for quantification of x-ray microtomography at the UGCT," *Nuclear Instruments and Methods in Physics Research A*, vol. 580, pp. 442–445, 2007.

[31] M. A. Beltran, D. M. Paganin, K. Uesugi, and M. J. Kitchen, "2d and 3d x-ray phase retrieval of multi-material objects using a single defocus distance," *Optics Express*, vol. 18, no. 7, pp. 6423–6436, 2010. [Online]. Available: http://dx.doi.org/10.1364/OE.18.006423

[32] M. A. Beltran, D. M. Paganin, K. W. Siu, A. Fouras, S. B. Hooper, D. H. Reser, and M. J. Kitchen, "Interface-specific x-ray phase retrieval tomography of complex biological organs," *Physics in Medicine and Biology*, vol. 56, no. 23, pp. 7353–7369, 2011. [Online]. Available: http://dx.doi.org/10.1088/0031-9155/56/23/002

[33] M. N. Boone, Y. De Witte, M. Dierick, A. Almeida, and L. Van Hoorebeke, "Improved signal-to-noise ratio in laboratory-based phase contrast tomography," *Microscopy and Microanalysis*, vol. 18, no. 2, pp. 399–405, 2012. [Online]. Available: http://dx.doi.org/10.1017/S1431927611012529

[34] B. D. Arhatari, W. P. Gates, N. Estiaghi, and A. G. Peele, "Phase retrieval tomography in the presence of noise," *Journal of Applied Physics*, vol. 107, no. 3, p. 034904, 2010. [Online]. Available: http://dx.doi.org/10.1063/1.3298930

[35] D.-J. Kroon, C. H. Slump, and T. J. Maal, "Optimized anisotropic rotational invariant diffusion scheme on cone-beam CT," *Med Image Comput Comput Assist Interv. (MICCAI)*, vol. 13, no. 3, pp. 221–228, 2010.

[36] J. Lindblad, N. Sladoje, and T. Lukic, "De-noising of SRμCT fiber images by total variation minimization," in *International Conference on Pattern Recognition (ICPR) 2010*. IEEE, 2010, pp. 4621–4624.